Dynamics of Sub-atmospheric Zones and Their Impact on the Fluid Flow and Heat Transfer Characteristics of Impinging Air Jet on Circular Standalone Ribbed Targets

5 authors, including:

Mohammed Khalifa
Kompetenzzentrum Holz GmbH
47 PUBLICATIONS   **705** CITATIONS

SEE PROFILE

Altaf Hussain Bagawan
SECAB Institute of Engineering and Technology, Vijayapur
4 PUBLICATIONS   **21** CITATIONS

SEE PROFILE

RESEARCH

Dynamics of sub-atmospheric zones and their impact on the fluid flow and heat transfer characteristics of impinging air jet on circular standalone ribbed targets

Vijaykumar Nagathan[1] · Mohammed Khalifa[2] · Altaf Hussain Bagawan[3] · Basavaraj M. Angadi[1] · Vadiraj Katti[1]

Abstract

Impinging jets are widely recognized for their exceptional heat transfer performance across various applications. Understanding the underlying principles of impinging jets is crucial for improving their effectiveness. In this study, an experimental investigation was conducted to evaluate the static pressure and heat transfer performance of a highly turbulent air jet on a standalone rib target surface. For this study, various parameters were considered, including rib diameters (8 mm to 28 mm), nozzle-to-plate spacing (H/D) (0.5-6.0), and Reynolds numbers (Re) ranging from 20,000 to 40,000. The results indicated that pressure and heat transfer distributions in the impinging jet strongly depended on H/D, Re, and rib diameter. The flow structure of the jet under detached ribs changed compared to the smooth surface, revealing complex flow behavior due to the formation of strong recirculation zones, which resulted in significant sub-atmospheric pressure regions. Consequently, heat transfer performance increased dramatically by 112% at the junction of this interplay, while an average heat transfer performance enhancement of 52% and a thermal performance factor of 1.63 was achieved using the standalone ribs compared to the smooth target surface. The heat transfer coefficients increased upon using the rib up to a diameter of 15 mm, after which a decreasing trend was observed. The optimum results were obtained with a rib diameter of 15 mm. This approach not only enhanced performance, but also opened new avenues for designing more effective cooling systems and improving the overall thermal management of engineering systems.

Graphical Abstract
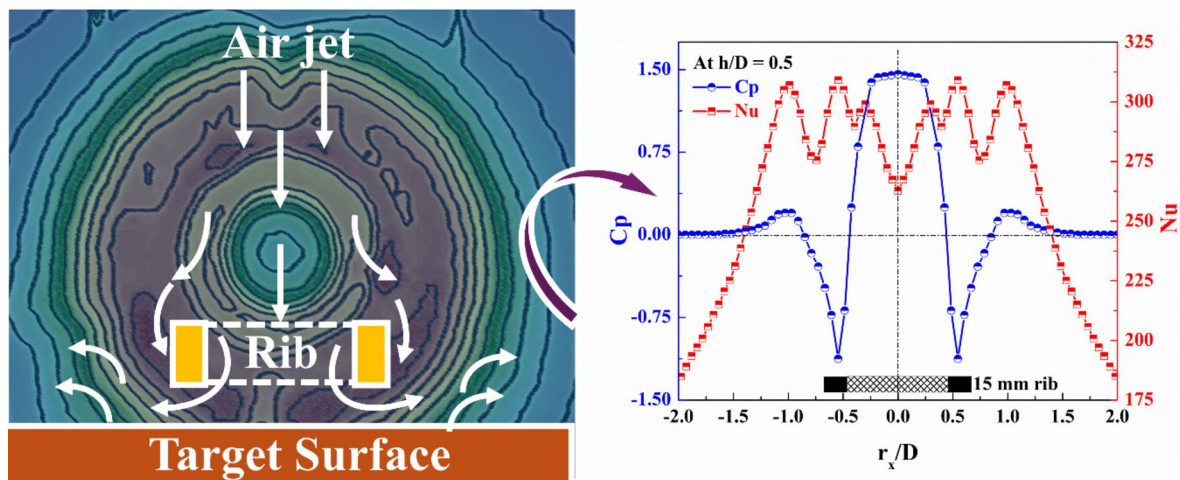
✉ Mohammed Khalifa
  m.khalifa@wood-kplus.at; mohammed.khalia89@gmail.com

1 B. L. D. E. A's V.P. Dr. P. G. Halakatti College of Engineering and Technology, Vijayapur, Karnataka, India

2 Kompetenzzentrum Holz GmbH, Altenberger Strasse 69, Linz 4040, Austria

3 Secab Institute of Engineering and Technology, Vijayapur, Karnataka, India

🖄 Springer

1 Introduction

Impinging jets have been adopted in various industries for efficient cooling of turbine blades, electronic components, billet cooling, engine cooling, solar panels etc. Impinging jet offers significant advantages including facile design and high heat transfer performance [1]. Heat transfer performance of impinging jets largely relies on various factors including flow behavior (laminar/turbulent), nozzle exit geometry, cooling surface area etc. On the other hand, jet configuration (single or array), distance with which the jet impinges on the cooling surface (H), jet temperature etc., affect the heat transfer performance. Since the turbulence enhances the heat removal capability, turbulent jets are considered appropriate for cooling applications [2–4]. Lytle and Webb [5] investigated the impact of low H-spacing on heat transfer characteristics in a circular air jet. They found that at low H-spacing (H/D < 0.25), the maximum Nusselt number (Nu) shifts from the stagnation point to a secondary peak, especially at higher Reynolds number (Re). To enhance turbulent intensity, various techniques can be employed, such as introducing detached ribs [6], vortex generators [7], turbulators [8], dimpled surfaces [9], perforated plates [10] and fins [11, 12]. These methods increase fluid mixing and turbulence, thereby improving heat transfer performance. Among them, the influence of a detached rib on fluid flow in an impinging jet is a topic of interest in fluid dynamics due to its relevance in heat transfer applications, cooling processes and aerodynamic studies. To develop an understanding of jet impingement heat transfer, it is essential to consider the nozzle geometry, flow confinement, target surface geometry and turbulence intensity at the nozzle exit [13, 14].

Previous studies indicated that jet impingement on a ribbed target surface disturbs the wall jet and enhances turbulence by promoting better fluid mixing, ultimately improving heat transfer [15]. A computational study was conducted to understand the influence of rectangular detached ribs on the local heat transfer distribution. The presence of detached ribs increased the heat transfer by 64% at H/D spacing 0.5 [16]. The utility of detached ribs has been found to offer better thermal performance than attached ribs by increasing the flow acceleration between the rib base and the target heated wall [17]. A simulated study revealed that the turbulence created by the ribs facilitated high local heat transfer rates [18]. Celik [19] reported that the utility of the co-axial jet and the roughened surface was found to enhance heat transfer by 27% compared to the circular air jet, with 6% of the enhancement contributed by the utility of the rough surface. A study explored fluid flow, heat transfer, and friction factors in a channel with various rib shapes. It was found that the v2-f model accurately predicted turbulent flow characteristics, with semi-circular ribs outperforming square ribs in heat transfer efficiency [20]. A computational model reported that the presence of detached ribs in the impingement channel had a notable impact on the flow field, potentially enhancing the overall Nu by 4% under adiabatic boundary conditions [21].

An experimental study was conducted to investigate the enhancement of heat transfer from a flat surface with a detached rib surface subjected to normal impingement by a circular jet. The study examined the effects of various parameters, including rib width, rib height and rib pitch on local heat transfer distribution. Compared to smooth surfaces, a consistent increase in Nu values was observed at the stagnation zone [22]. An experimental study examined the effects of a confined slot jet impinging on a ribbed rough surface at a Re of 2500. The results showed that maximum wall static pressure was observed at the stagnation point, which decreased with an increasing H/D ratio. A sub-atmospheric pressure was observed at low H/D ratios for all rough surfaces. The highest Nu was found at the stagnation point, with a 4 mm rib [23]. In another study, circular ribs were positioned at the geometric center and tested with different radii and heights. It was found that the rib height that best matched the velocity boundary layer thickness at its location was the most effective for maximizing heat transfer. However, an excessive increase in rib height resulted in lower heat transfer rates than a smooth target surface. Additionally, placing the rib in the stagnation region was ineffective in improving heat transfer regardless of rib height [24]. Using a single jet is the most common method of jet impingement and represents a good starting point for comparing the augmentation of the system. With a single jet, it is possible to change various parameters to examine the system's potential heat transfer performance. The influence of a detached rib on an impinging jet involves a complex interplay between flow separation, turbulence generation, and momentum redistribution. The net effect depends on the rib size, shape, position relative to the jet, and the Re of air exiting the jet. Understanding these parameters is critical in optimizing systems that utilize impinging jets for cooling, heating, or aerodynamic applications.

Despite numerous studies on the impact of detached ribs, there is a lack of research examining how different rib sizes affect wall static pressure distribution in impinging air jets and their influence on recirculation and sub-atmospheric zones. Most existing research relies on computational methods and focuses on low Re. Since turbulent fluid dynamics play a crucial role in impingement cooling, understanding these dynamics is essential for optimizing heat transfer. This study aims to experimentally investigate the effects of rib sizes on wall static pressure distribution and subsequently assess their impact on heat transfer performance. Experiments were conducted with rib sizes ranging from 8 mm to
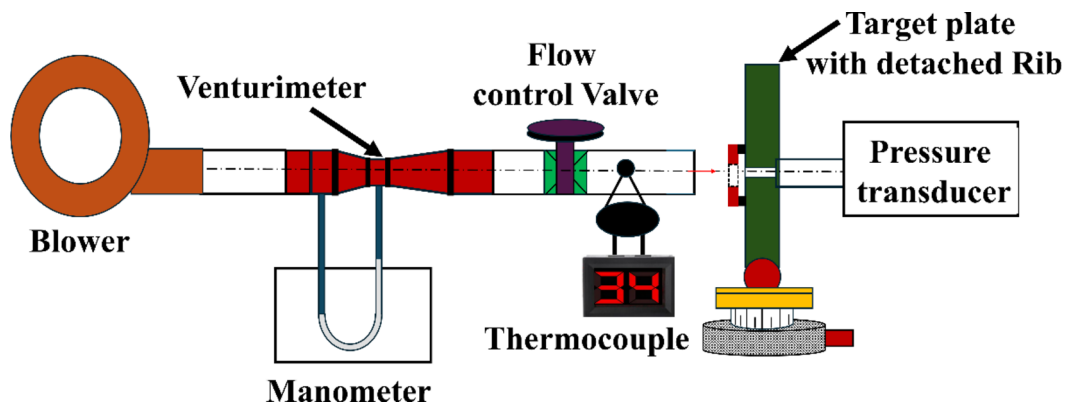
Fig. 1 Schematic depiction of experimental setup fabricated indigenously for fluid flow studies

Fig. 2 Test setup used to evaluate heat transfer characteristics of the impinging jet
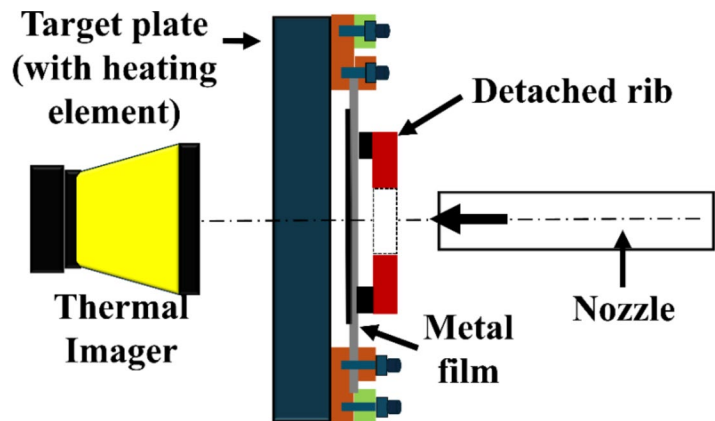
28 mm and various H/D spacings. Additionally, tests were performed to evaluate the effect of Re on fluid flow and heat transfer performance. Besides, the results were compared with those from smooth target surfaces to comprehensively analyze rib size effects on static pressure distribution and heat transfer characteristics.

2 Experimental setup

A horizontal-axis impinging jet setup was fabricated indigenously in our laboratory to evaluate the effect of detached ribs on the fluid dynamics and heat transfer performance of an axisymmetric air jet (Fig. 1). Air was discharged at the desired Reynolds number (Re), regulated precisely using a combination of a regulator valve and a Venturi meter connected to a U-tube manometer. A long aluminum nozzle with an inner diameter of 16.5 mm and a length of 750 mm was employed to ensure a fully developed turbulent flow. The temperature of the air near the nozzle exit was continuously monitored using a K-type thermocouple. An acrylic target plate (250 mm ×250 mm ×10 mm) was used to evaluate the fluid flow characteristics. The static pressure distribution was measured with a Ø0.5 mm pressure tap made on the target plate to yield the pressure change data. The target

plate was mounted on a high-precision traversing table, allowing controlled movement in the axial direction for spatial resolution of the flow field. A digital pressure transducer was also connected via a pressure tap to capture real-time pressure variations during fluid flow studies.

Cp was calculated using the following equation:

$$Cp = \frac{\Delta P}{0.5 \times \rho \times V_j^2} \tag{1}$$

Where, ΔP = pressure change on the target surface; V_j: average velocity of air at the nozzle exit; and ρ = air density.

Furthermore, a similar setup was used to determine the heat transfer characteristics, except for the target surface, which was fabricated using the procedure outlined in our previous studies [3] (Fig. 2). The target surface made of steel foil painted with black color having an average emissivity of 0.97, which was measured experimentally as described in our previous studies [25]. A thermal imager [Fluke Ti 55 IR Fusion Technology, USA] was utilized to capture the temperature distribution over the surface. For heat transfer experiments, the temperature of the target surface was regulated by adjusting the electrical power supplied to embedded copper bus bars. This was achieved using a voltage regulator (Meco Instruments, India) to maintain

desired surface temperatures. The Nusselt (Nu) number was determined using the following Eq.

$$N_u = \frac{hd}{k} \qquad (2)$$

Where,

$$h = \frac{q_{conv}}{T_r - T_j} \qquad (3)$$

$$q_{conv} = \frac{q_j - q_{loss}}{T_r - T_j} \qquad (4)$$

$$q_j = \frac{VI}{A} \qquad (5)$$

Where, h: heat transfer coefficient (W/m^2 K); k: thermal conductivity of air (W/m K); T_j: jet temperature (°C); T_r: Temperature of the target plate in radial directions (°C), q_{conv} is net heat flux; q_{loss}: Heat flux loss due to radiation and natural convection; q_j is ohmic heat flux; V and I are voltage (V) and current values (A), respectively.

Thermal performance factor (TPF) was determined using the following Eq.

$$TPF = \frac{Nu/Nu_b}{f/f_o}. \qquad (6)$$

and

$$f = \frac{2 \times \Delta P}{\rho \times U_{avg}^2} \qquad (7)$$

Where, ΔP =change in static pressure; ρ= Density; U_{avg} = Average velocity at jet exit, Nu_b = Nu values of smooth surface considered as reference; f and f_o are the friction factor with and without detached ribs, respectively.

The pressure and temperature distribution were measured at various distances between the jet exit and the target surface (H) and radial spreading (r_x). Furthermore, Re was maintained at 40,000 to ensure high air turbulence. Axisymmetric detached ribs with varying diameters (Ø8–28 mm) were positioned 1 mm above the target surface. Brackets were adhesively bonded to the rib width to ensure a secure attachment. Spacers were affixed to the target surface, maintaining a uniform gap of 1 mm and located at least 30 mm away from the working zone to avoid interference. The height and width of all ribs were consistently maintained at 3.45 ±0.03 mm. A digital image and schematic illustration of rib attachment to the target plate is illustrated in Fig. 3. For simplicity, the values of "H" and "r_x" are expressed as non-dimensional numbers as H/D (0.5–6.0) and r_x/D (0–4.0).

The uncertainty analysis for the measurements in the air jet impingement setup accounts for uncertainties from multiple sources. This analysis followed the procedure described in previous studies [22, 26]. A detailed methodology is presented in the supplementary information (ESI. S1).

3 Results and discussion

3.1 Pressure distribution studies

Initially, experiments were conducted to assess the relationship between Re and Cp for smooth and ribbed surfaces in an impinging turbulent air jet. The tests aimed to determine the influence of Re on Cp distribution. Understanding the dependency between Re and Cp is crucial in fluid dynamics, as it helps predict flow characteristics and their associated
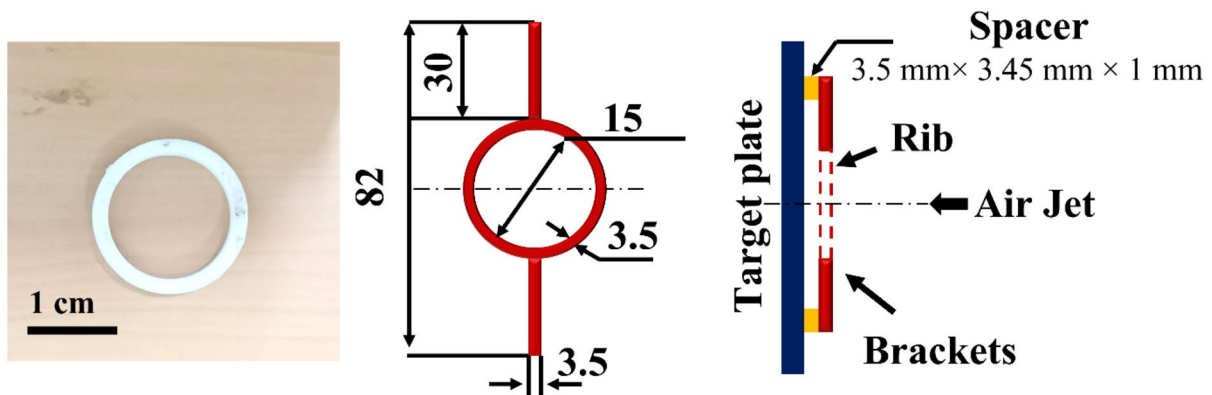
Fig. 3 Digital photograph and schematic of detached rib illustrating the brackets attached to the rib

heat transfer behavior. It is a well-understood phenomenon that when Cp is independent of Re, the analysis and design process is relatively straightforward. In contrast, when Cp depends on Re, the process becomes more complex, as the flow characteristics such as turbulence, boundary layer development, and flow separation vary with changes in Re, requiring more detailed and sophisticated models. The experiments were conducted at a Re of 20,000, 30,000, and 40,000. Figure 4a and b show the Cp distribution at different Re for smooth and ribbed target surfaces, respectively. The test was conducted at a specific H/D value of 0.5 as a function of r_x/D. For the smooth target surface, it was observed that the Cp remained constant across different Re, indicating that Cp is independent of Re. In a turbulent regime, the pressure distribution becomes stable and is primarily influenced by the jet geometry and overall flow dynamics and Cp remains largely constant, regardless of variations in Re. In contrast, for the ribbed surface, Cp exhibited a clear dependency on Re. A noticeable variation in Cp was observed with varying Re. At the stagnation point, Cp decreased as Re increased and remained consistent with r_x/D. Beyond $r_x/D = 1.25$, the dependence lessened, and all the curves overlapped, indicating a weak dependency of Cp on varying Re beyond an r_x/D of 1.25. It is further important to note that the sub-atmospheric pressure zones became stronger as Re increased. The dependency of Cp on Re could be attributed to the complex flow interactions introduced by the positioning of the detached ribs, which makes the flow regime more sensitive to the geometry of the target surface.

Additionally, a comparison was made to validate and correlate our findings with the previous studies conducted and published elsewhere (Fig. S2) (See ESI. S2). The test was carried out at H/D spacing of 1.0 and Re of 20,000, aligning with the conditions used in the previous studies [22]. The results suggest strong agreement with the previous findings,

confirming the reliability of our indigenously built test setup and analytical approach.

Since, the sub-atmospheric pressure was significant at higher Re; therefore, further studies were conducted at 40,000 Re. Figure 5a-f shows the Cp distribution as a function of r_x/D for smooth and ribbed target surface with varying diameters of detach ribs (8 mm, 10 mm, 12 mm, 15 mm and 28 mm). For a smooth target surface, the Cp values in the vicinity of the stagnation zone were observed to be higher across all H/D ratios, progressively decreasing with an increase in the H/D ratios.

As the jet approaches the target, it experiences deceleration, resulting in a noticeable Cp distribution at the stagnation point. The Cp values gradually weaken as the jet expands radially until reaching a saturation value of 0.0, which remains constant with further radial expansion of the jet. This could be attributed to the fact that the air spreads radially outward from the stagnation zone, expanding over a larger area, leading to a loss of flow momentum [27]. Furthermore, overall Cp values decreased as the H/D ratio increased. For a better understanding of the effect of ribbed surfaces, a comparison is shown in Fig. 6 depicting the formation of sub-atmospheric zones in ribbed targets.

In the case of ribbed surfaces, the pressure distribution was distinctly different from that of the smooth target surface. Figure 7a shows stagnation pressure at various H/D ratios for smooth and ribbed targets. Near the stagnation zone, the Cp was higher than that of the smooth target surface, which could be attributed to the sharp deceleration of the jet, leading to a build-up of pressure [28]. This suggests that the ribs create obstacles for the impinging jet in the stagnation zone. Furthermore, a strong sub-atmospheric zone formed near the width of the rib and became stronger as the rib diameter increased up to 15 mm due to the disturbance in the flow regime caused by the presence of
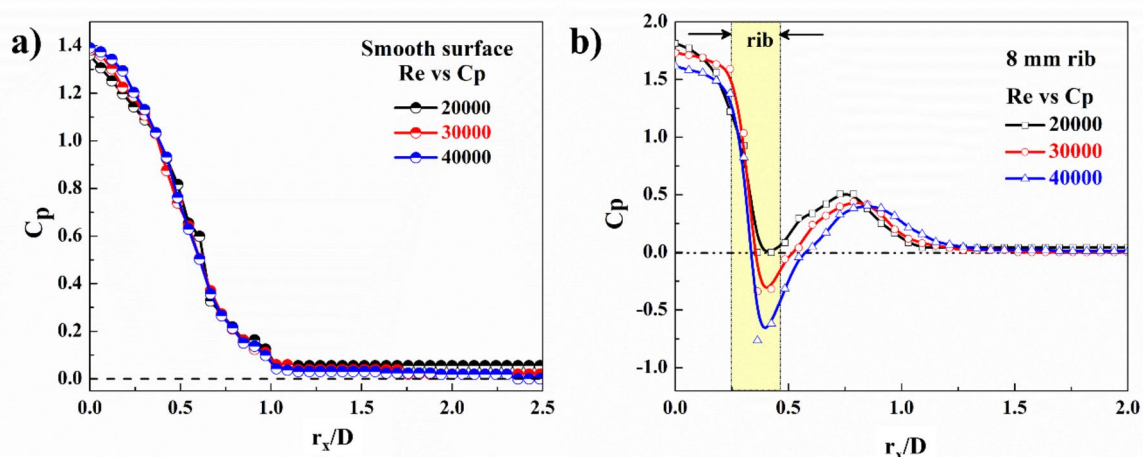

Fig. 4 Independence test to study the influence of Re on Cp as a function of H/D = 0.5; (**a**) Smooth target surface; (**b**) Ribbed target surface
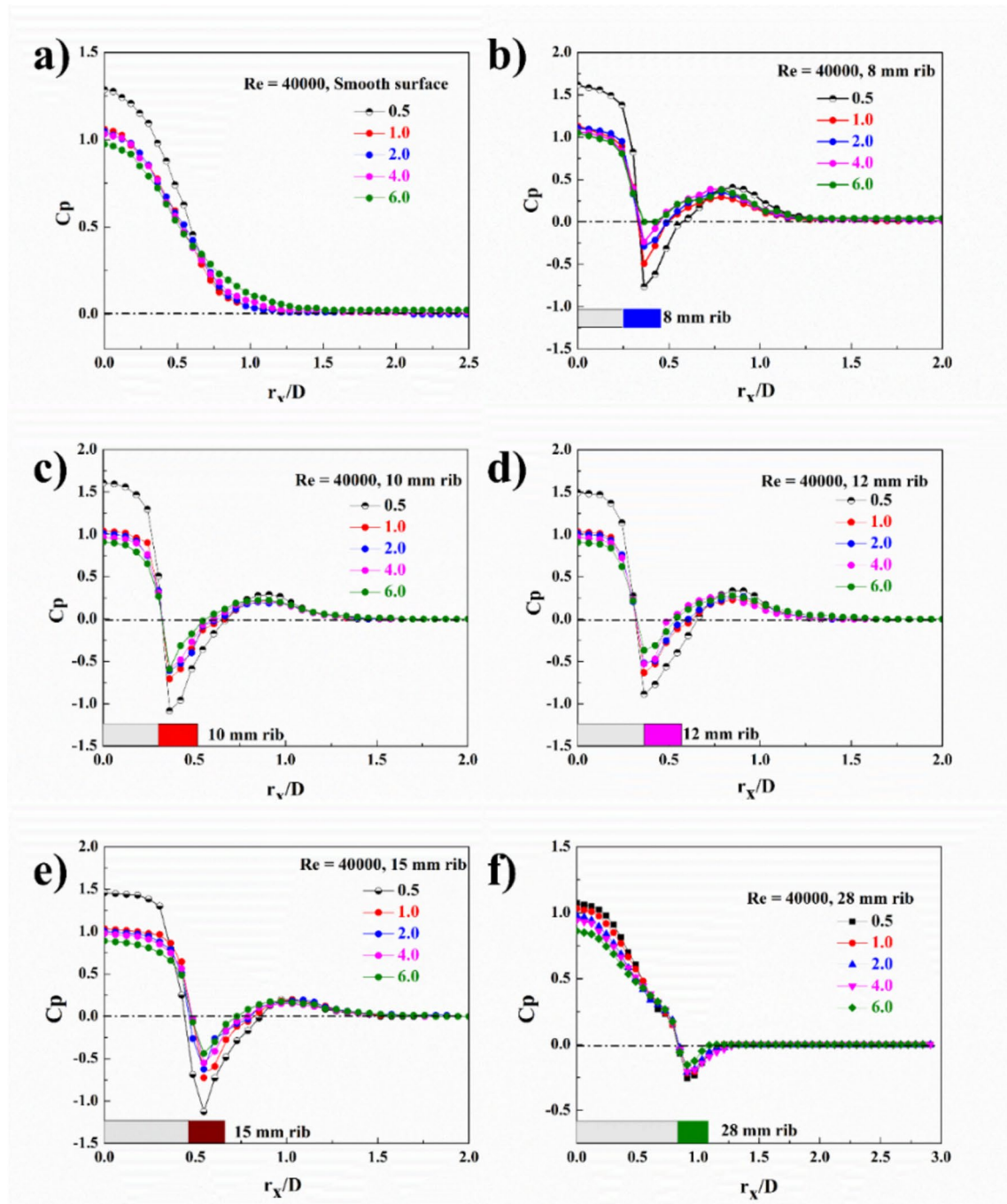
Fig. 5 Static pressure distribution at different H/D ratios for target surfaces with (**a**) smooth surface; (**b**) 8 mm rib; (**c**) 10 mm rib; (**d**) 12 mm rib; (**e**) 15 mm rib; (**f**) 28 mm rib

detached ribs. When the jet impinges on the ribbed target plate, a part of the jet flow may underpass the rib structure, separating from the surface at the rib edge, creating a recirculation zone or vortices downstream of the rib. Furthermore, the flow disruption at the rib edge and the subsequent recirculation causes a localized suction effect, leading to a sub-atmospheric pressure region [29–32]. Additionally, the curves indicated that the sub-atmospheric pressure zones are

generally stronger at the width of the rib, where flow separation is significant. The sub-atmospheric zone was found to be sensitive to the rib diameter and H/D ratio (Fig. 7b). A sub-atmospheric zone was observed for all H/D values across all ribs considered and became significant with increasing the rib diameter. The formation of a sub-atmospheric zone could be attributed to the pronounced separation and strong vortices formed immediately downstream of the jet, which
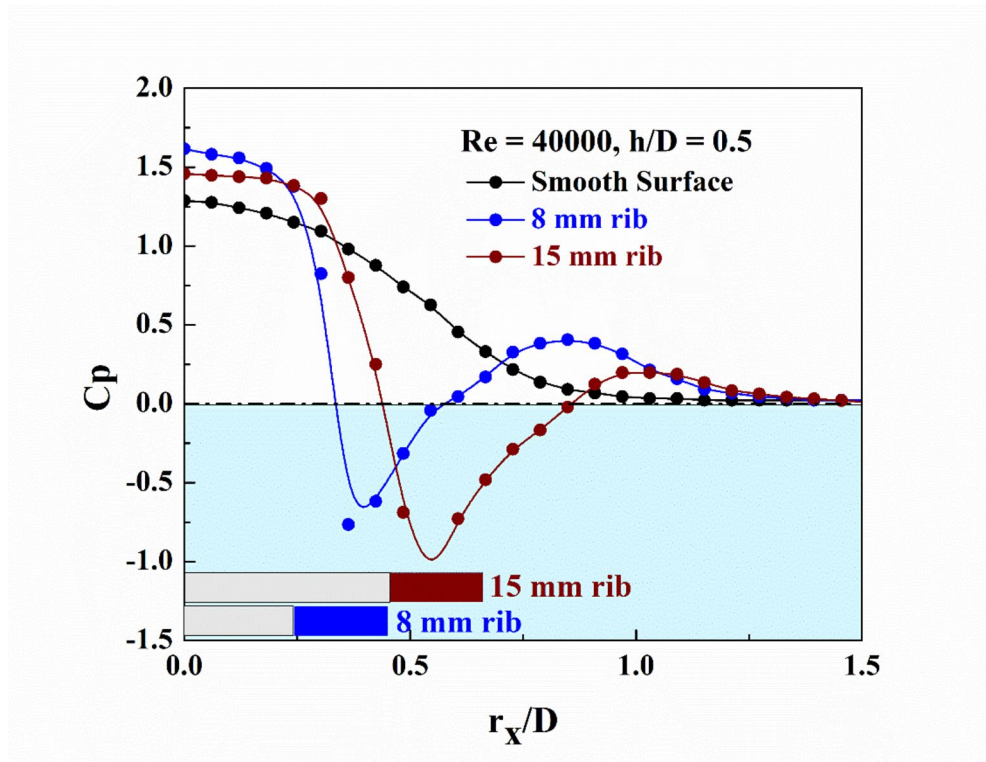
**Fig. 6** Comparison of Cp for smooth and ribbed surfaces at a H/D ratio of 0.5

could have resulted in strong sub-atmospheric zones as the air wriggles to reattach quickly, creating localized large vortices. However, when the rib diameter exceeds the diameter of the nozzle, the sub-atmospheric zone weakens, which may be linked to the wider spread of the jet and a reduction in the strength of the vortex or recirculating zones. For a 28 mm rib, the rib edge is situated beyond the stagnation zone, allowing the flow to reattach and recover easily, leading to a loss of the necessary momentum for the formation of sub-atmospheric zones.

Figure 7c shows the normalized static pressure distribution $1 - \frac{Cp}{Cp_0}$ as a function of r_x/D signifies an insight into the static pressure variations with different target surfaces in impinging air jet scenarios. The normalized pressure values increased progressively for a smooth surface as the jet spread radially outwards. This indicates that the flow experiences a steady pressure drop, eventually reaching a saturation value of 1, indicating that the flow was stabilized, with minimal changes in pressure. On the other hand, an abrupt rise in the slope was observed for ribbed target surfaces, indicating a stronger flow acceleration and a sharp decline in static pressure. This could be attributed to increased turbulence due to ribbed surfaces. Such flow regimes are important as they facilitate intense mixing and high transfer performance in the near-wall region. Further, as the jet spreads radially, the value reaches 1, indicating the flow has developed uniformly and the effect of the rib diminishes.

This analysis helps to understand and establish a strong relationship between fluid flow and heat transfer characteristics.

One interesting finding from this work was that the total radial distance over which the influence of the ribs (up to 15 mm) was detected consistently matched the diameter of the nozzle. This consistent pattern suggests a strong correlation between rib geometry, nozzle size and the distribution of pressure fields, particularly under conditions of proximity between the jet exit and the target surface. This observation also indicated that the nozzle diameter is vital in determining the flow disturbance caused by the detached ribs. Another finding from this study was observed at an H/D ratio of 0.5 for all detached ribs. Specifically, the radial distance from the point of initiation of negative pressure to its recovery to atmospheric pressure (where the pressure coefficient, Cp =0) was found to be approximately equal to the radius of the corresponding rib. This phenomenon occurred exclusively when the H/D ratio was small (H/D <0.5) (Fig. 7d and Fig. S3). However, the exact phenomenon behind this trend remains unclear. Moreover, to the best of our knowledge, there are no previous studies discussing this specific trend in the literature. Ideally, we believe that this phenomenon, where the pressure recovers to atmospheric levels at a distance equal to the rib radius, could be attributed to the interplay between the flow separation caused by the ribs and the subsequent reattachment of the flow. As the flow interacts with the ribbed surface, the separation and subsequent
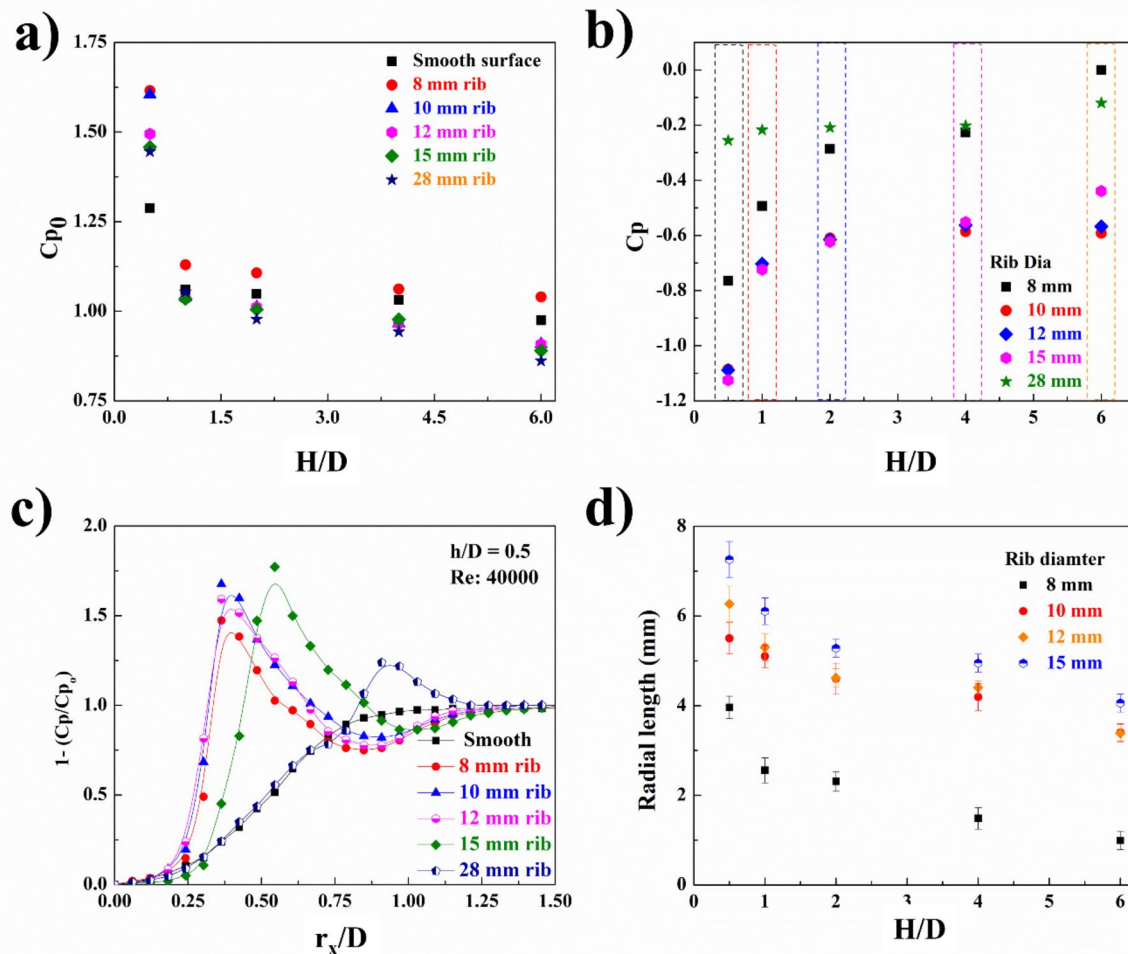
Fig. 7 (**a**) Stagnation pressure at different H/D ratio for smooth and ribbed targets; (**b**) Maximum negative pressure values observed at different H/D ratio for ribbed targets; (**c**) Normalized Pressure Distribution Variation of as a function of r_x/D for different ribbed surfaces; (**d**) Sub-atmospheric pressure zone of jet along radial direction for different ribbed targets

recirculation zones contribute to this particular pressure distribution pattern. The pronounced effect at small H/D ratios further highlights the sensitivity of the flow dynamics to the spacing between the jet exit and the target surface.

4 Heat transfer studies

Heat transfer studies were conducted to determine the influence of detached ribs on heat transfer performance and to establish a relationship between fluid flow and heat transfer characteristics. The influence of rib configurations on the Nu at different H/D ratios is illustrated in Fig. 8 (a-f). Among all configurations, the highest Nu values were achieved at a lower H/D ratio (0.5) and gradually decreased as the H/D ratio increased. Additionally, the Nu values were sensitive to rib diameter, with the values increasing as the rib diameter increased up to 15 mm, beyond which a decreasing trend

was observed. For smooth surface conditions, the highest Nu values appeared around the stagnation region and gradually decreased as the jet spread radially with a secondary peak observed around the r_x/D value of 1.25–2.25. This secondary peak could be attributed to the development of a localized turbulence region in the boundary layer as the jet exited radially and was distinctly observed at higher Re (Re >20000) and lower H/D ratios (H/D <4.0).

Contrary to the trends of smooth surface (*Nu values decrease gradually as the jet spreads radially*), target surfaces with detached ribs exhibited lower Nu values around the stagnation point and increased as the jet spread across the width of the rib. However, the Nu values on all ribbed surfaces were higher than those on smooth surfaces. At H/D =0.5, the Nu at the stagnation point (Nu_0) ($r_x/D =0$) was 172 for smooth surface, which dramatically increased by 38%, 39.5%, 46.5%, and 52.3% for ribbed target surfaces with 8 mm, 10 mm, 12 mm, and 15 mm ribs, respectively (Fig.
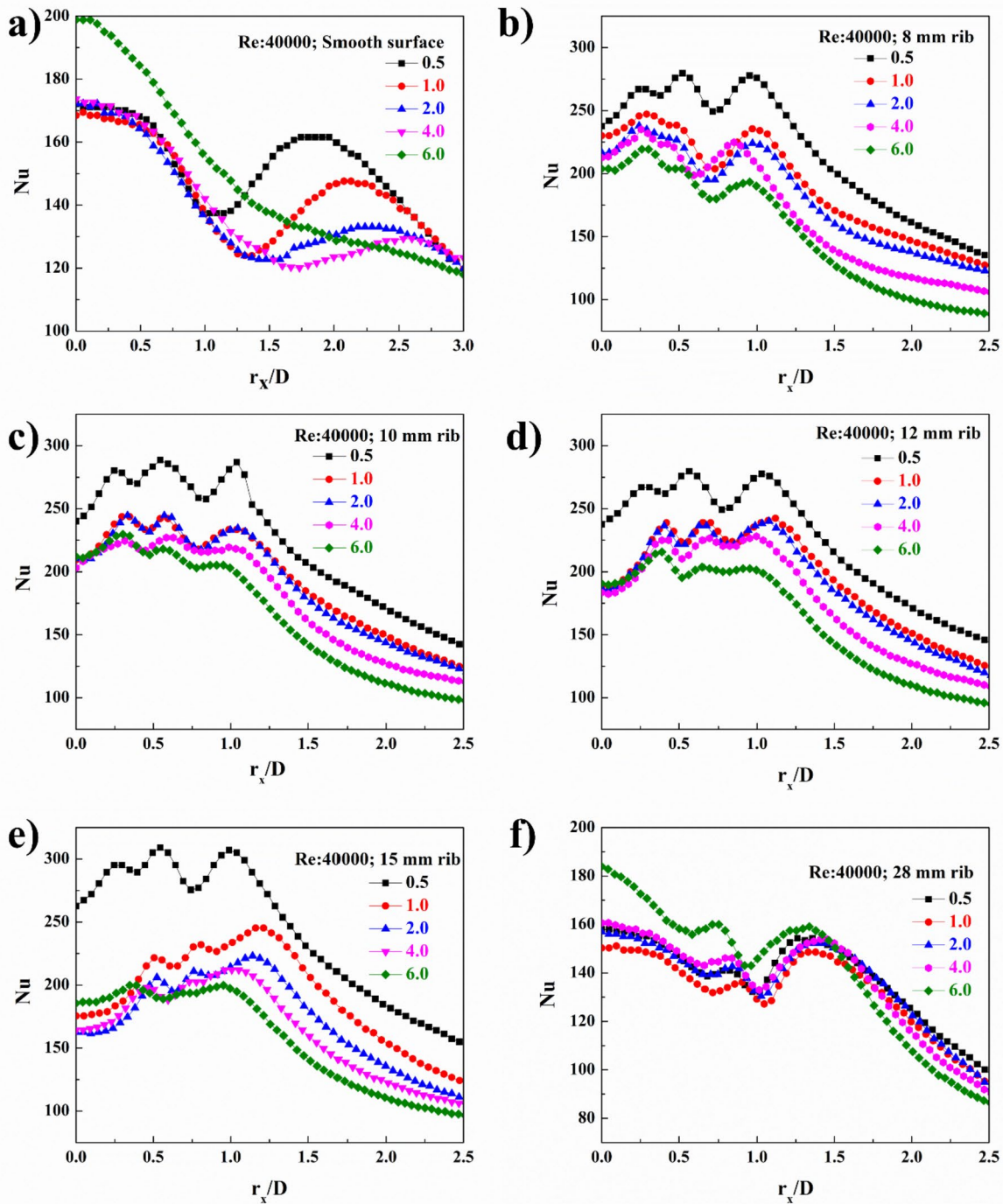
Fig. 8 Nu number distribution at different H/D ratios for target surfaces with (**a**) smooth surface; (**b**) 8 mm rib; (**c**) 10 mm rib; (**d**) 12 mm rib; (**e**) 15 mm rib; (**f**) 28 mm rib

S4) [See ESI S3]. However, there was a 9% decrease for a rib configuration of 28 mm. The highest Nu value of 310 (r_x/D =1.3) was observed for 15 mm ribbed surfaces at an H/D ratio of 0.5, which is approximately 112% higher than that of the smooth surface. Overall, an average increase of

52% in the heat transfer coefficient was observed when the target surface was configured with detached ribs.

Moreover, three distinct Nu peaks were observed on ribbed surfaces, with their locations depending on rib diameter, rib width and H/D ratio. Based on these observations,

the jet flow over the target surface can be divided into five distinct zones as shown in Fig. 9.

Zone 1 The jet impinges on the ribbed target surfaces, where it decelerates and the velocity decreases dramatically. In this zone, Cp values were higher as the jet impinged on the target.

Zone 2 As the air flows radially from zone 1 to zone 2, located just before the inner wall of the rib surface, the pressure decreased abruptly and the jet gains the necessary velocity, resulting in high turbulent intensity. This leads to the formation of a strong recirculation zone and vortices, resulting in a localized increase in Nu values.

Zone 3 As the jet passes from zone 2 to zone 3, it moves through the clearance between the rib and the target surface. The static pressure decreased further, leading to another peak in the Nu due to the maximum intensity of turbulence in this region, as confirmed by static pressure distribution studies.

Zone 4 Another Nu peak was observed as the jet moves from the outer wall of the rib (zone 3 to zone 4). However, this peak was weaker than that in zone 3 since most of the heat had already been removed by the jet passing through zones 1–3. Nevertheless, in this zone the pressure was recovered as the air started to spread outwards without any obstacles, but hitherto sufficient turbulence persisted to form another peak.

Zone 5 As the jet transits from zone 4 to zone 5, the Nu values decreased dramatically as the jet spreads radially outward over a large surface area. This spreading causes the jet to lose the necessary momentum, reducing its convective heat transfer capability.

A strong correlation was observed between Cp and Nu, with significant increases or decreases in Nu values corresponding to dramatic variations in Cp. This relationship highlights the intrinsic link between fluid flow dynamics and convective heat transfer capability. In regions where Cp drops significantly, it often signals increased turbulence and flow velocity, both of which enhance the convective heat transfer process. Turbulence increases the mixing of fluid near the target surface, disrupting the thermal boundary layer and facilitating more efficient heat transfer. Conversely, areas with low velocity and low turbulence resulted in thicker thermal boundary layers and reduced heat transfer rates. Moreover, the peaks observed on ribbed surfaces were sensitive to rib diameter and shifted radially outward as rib diameter increased. In contrast, the Nu dramatically
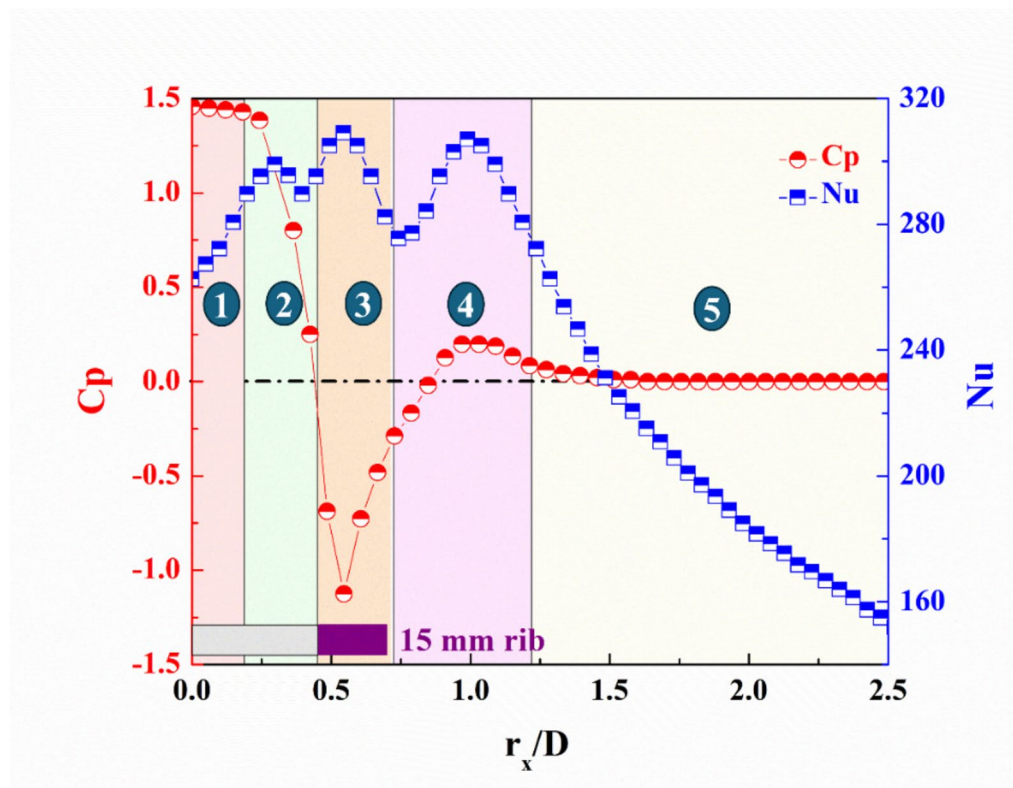
Fig. 9 Different zones of Static pressure and heat transfer distribution at a H/D spacing of 0.5 for a ribbed target surface with 15 mm rib

Table 1 Shows the TPF of an impinging air jet on target surfaces across varying diameters of detached ribs

Rib Diameter (mm)	TPF
0	
8	1.34 ±0.03
10	1.4 ±0.03
12	1.45 ±0.022
15	1.63 ±0.035
28	0.91 ±0.034

Table 2 Comparison of this study with previously published results

Rib configuration	Jet type	Study	% Nu enhancement	Ref.
Detach ribs (rectangular)	circular	Computational	64%	[16]
Dimple surface	Co-axial jet	Experimental	27%	[19]
Detach ribs (Square)	Multiple jet	Experimental	4%	[21]
Detach ribs (triangular ribs)	circular	Experimental	22.8%	[33]
Detach ribs (Circular)	circular	Numerical	7%	[18]
Detach ribs (Circular)	circular (single, multiple and crossflow)	Computational	11%	[34]
Detach ribs (Circular)	Axisymmetric	Experimental	~ 70%	[22]
Perforated ribs	multiple circular jet array	Experimental	48%	[10]
Detached ribs (circular)	**Single circular jet**	**Experimental**	**112%**	**This study**

decreased for the 28 mm rib diameter. This could be attributed to the fact that the jet had sufficient space to spread radially without interference, resulting in weak turbulence, consistent with fluid flow studies. Additionally, the rib location away from the jet impingement point led to a loss of necessary jet momentum. It is also important to note that the Nu values were higher when the rib diameter was smaller than the nozzle diameter and decreased as the rib diameter exceeded the nozzle diameter. This can be explained by the fact that smaller rib diameters allow for more concentrated and directed jet impingement, which enhances localized heat transfer, while larger diameters disperse the jet over a broader area, diminishing the overall impact on the target surface.

Overall, the presence of detached ribs created large velocity variations, particularly in zones 2, 3, and 4, resulting in effective mixing due to vortices, whirling effects and wake formation behind the ribs [10–12]. Furthermore, thermal performance factor (TPF) was determined by considering the smooth target surface as the baseline. Table 1. shows the

TPF of the impinging air jet on target surfaces across varying diameters of detached ribs. The results confirmed a clear increasing trend in TPF as the rib diameter increased. Specifically, increasing the rib diameter from 8 mm to 15 mm, TPF improved progressively from 1.3 to 1.63. However, for a 28 mm rib, the TPF decreased to 0.91. This suggests that detached ribs enhance heat transfer efficiency, overcoming friction losses and improving thermal performance. The observed trend highlights that selecting a detached rib diameter close to the nozzle diameter is recommended for optimal thermal performance.

Table 2 shows the comparison of the present study with the results from the literature. Although other parameters, such as rib clearance, height, width and thickness, may also play a role in influencing the heat transfer values [3]. Furthermore, the observed variations in Nu peaks across different zones suggest that optimizing rib geometry and its location is crucial, particularly in applications requiring precise control of local thermal conditions.

Figure 10a-d shows the contour maps of Nu distribution at a H/D =0.5 for different rib configurations (smooth surface, 8 mm, 15 mm and 28 mm). At the stagnation point, the shape of jet impingement shows different shapes from circular to irregular, indicating a diversity in flow conditions including surface geometry and jet characteristics. On smooth surfaces, the contour lines are more dispersed, indicating a gradual change in Nu values as the jet spreads radially. This gradual change can be attributed to steady variations in the fluid flow characteristics across the surface. In contrast, the contour lines are closely spaced for ribbed surfaces, suggesting a rapid change in Nu values over a small radial distance. This is likely due to the formation of strong turbulent regions or steep thermal gradients associated with high-velocity areas around the ribs [13–15].

As the jet spreads radially outward, more contour lines appear on ribbed surfaces, indicating localized areas of enhanced heat transfer. The dense contour maps confirm the complex flow dynamics introduced by the presence of standalone ribs on the target surface. However, this dense clustering of contour lines also showed that the high heat transfer rates quickly diminish as the distance from the center increases. Additionally, for a rib diameter of 28 mm, the contour map exhibited a pattern similar to that of a smooth surface, suggesting that the ribbed configuration in this case did not significantly disrupt the flow or enhance heat transfer. These observations are consistent with the trends discussed in previous sections, reinforcing the correlation between surface geometry, flow dynamics, and heat transfer performance. Moreover, at H/D =6.0, a similar observation has been made, wherein for ribbed surface contour lines are closely spaced, indicating high heat transfer rates compared to surfaces without detached ribs (Fig. 11a-b).
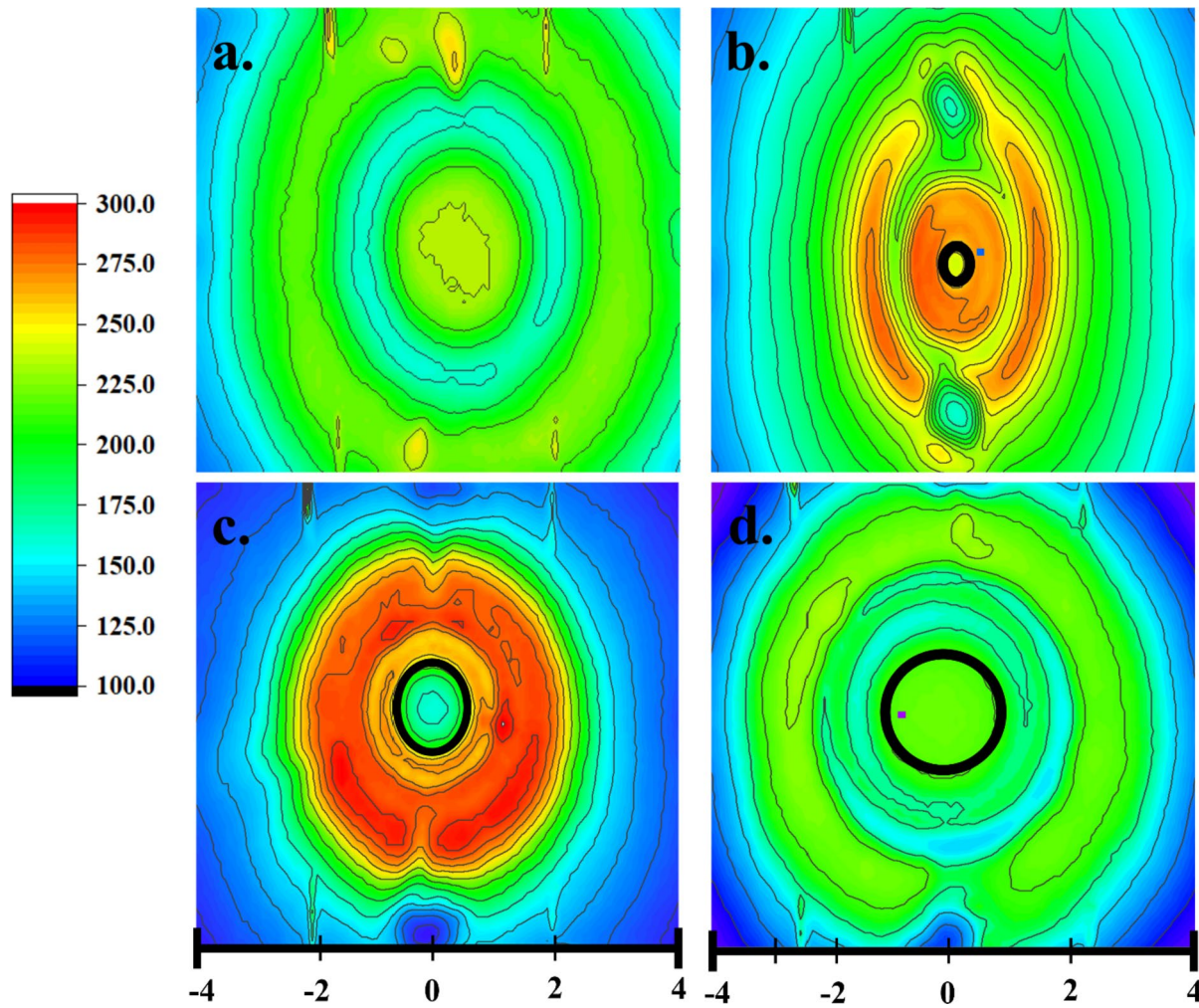
Fig. 10 Contour mapping of Nu for different rib configurations at H/D ratio of 0.5 (**a**) smooth surface; (**b**) 8 mm rib; (**c**) 15 mm rib; (**d**) 28 mm
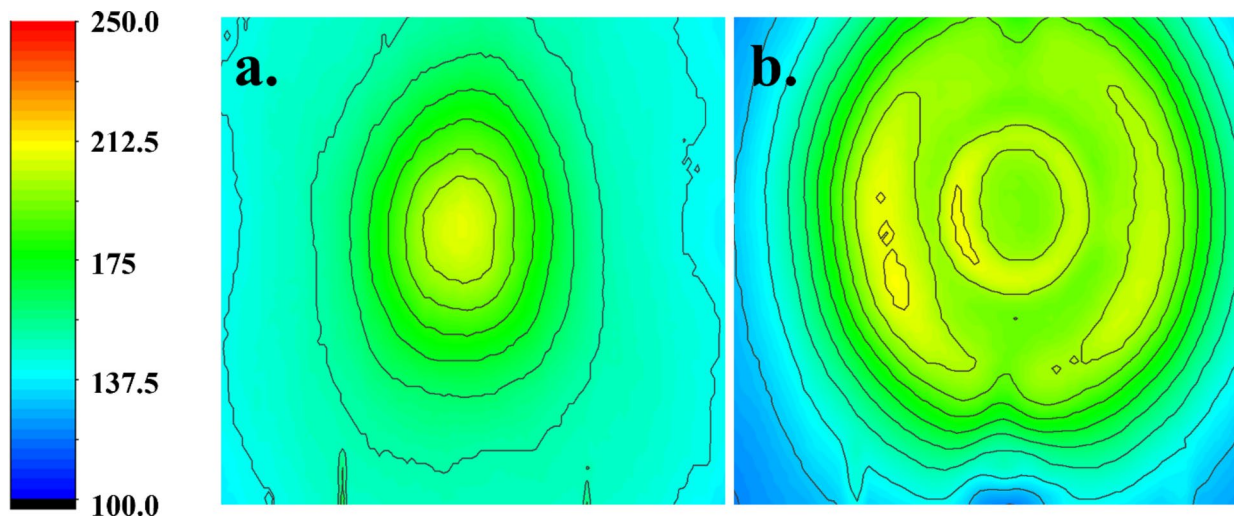

Fig. 11 Contour mapping of Nu numbers at H/D ratio of 6.0 (**a**) smooth surface; (**b**) 15 mm rib

5 Conclusion

A comprehensive investigation explored the impact of axisymmetric detached ribs on the static pressure coefficient (Cp) and heat transfer coefficients (Nu) of an impinging circular air jet. The study examined several parameters, including rib sizes, axial distance (H/D), radial distance (r_x/D), and Reynolds number (Re), to understand their effects on fluid dynamics and heat transfer performance. The findings revealed that the configuration of the detached ribs, Re number and H/D ratio significantly influenced the pressure distribution and heat transfer characteristics. The presence of detached ribs disrupted the jet flow, generating strong recirculation zones and inducing a whirling effect, which led to the formation of sub-atmospheric pressure regions. These phenomena were closely linked to the interaction between rib configuration, jet flow, and nozzle diameter. Consequently, the Nu values were substantially higher on surfaces with detached ribs than those on smooth surfaces. Notably, local heat transfer performance improved by 112% in regions with sub-atmospheric pressure, while an overall enhancement of 52% was observed for surfaces with detached ribs relative to smooth surfaces. Overall, this study not only investigated the effect of detached ribs on impinging jets, but also provided a comprehensive understanding and correlation of fluid flow and heat transfer characteristics. On the other hand, studies related to other factors, such as rib location in the radial direction, rib clearance, rib width, and mounts with different target geometries, are essential for further understanding and optimizing the heat transfer performance of impinging jets.

Declarations

References

1. Cho HH, Kim KM, Song J (2011) Applications of impingement jet cooling systems. In: Shanley AI (ed) Cooling systems: energy, engineering, and applications. Nova Science, Inc, pp 37–67
2. Barewar SD, Joshi M, Sharma PO et al (2023) Optimization of jet impingement heat transfer: A review on advanced techniques and parameters. Therm Sci Eng Prog 39
3. Yalçınkaya O, Durmaz U, Tepe AÜ et al (2023) Thermal performance of elliptical pins on a semicircular concave surface in the staggered array jet impingement cooling. Appl Therm Eng 231
4. Yalçınkaya O, Durmaz U, Tepe AÜ et al (2022) Effect of slot-shaped pins on heat transfer performance in the extended jet impingement cooling. Int J Therm Sci 179
5. Lytle D, Webb BW (1994) Air jet impingement heat transfer at low nozzle-plate spacings. Int J Heat Mass Transf 37:1687–1697. https://doi.org/10.1016/0017-9310(94)90059-0
6. Kong D, Chen W, Niu X et al (2024) A comparative study of internal heat transfer enhancement of impingement/effusion cooling roughened by solid rib and Slit rib. Phys Fluids 36. https://doi.org/10.1063/5.0179254
7. Nakod PM, Prabhu SV, Vedula RP (2008) Heat transfer augmentation between impinging circular air jet and flat plate using finned surfaces and vortex generators. Exp Therm Fluid Sci 32:1168–1187. https://doi.org/10.1016/j.expthermflusci.2008.01.009
8. Wang Z, Zhang Q, Yan Y et al (2017) Secondary flows and extra heat transfer enhancement of ribbed surfaces with jet impingement. Numer Heat Transf Part Appl 72:669–680. https://doi.org/10.1080/10407782.2017.1394139
9. Kanokjaruvijit K, Martinez-Botas RF (2005) Jet impingement on a dimpled surface with different crossflow schemes. Int J Heat Mass Transf 48:161–170. https://doi.org/10.1016/j.ijheatmasstransfer.2004.08.005
10. Caliskan S (2013) Flow and heat transfer characteristics of transverse perforated ribs under impingement jets. Int J Heat Mass Transf 66:244–260. https://doi.org/10.1016/j.ijheatmasstransfer.2013.07.027
11. Yalçınkaya O, Özel Mb, Durmaz U, Uysal Ü (2024) Experimental heat transfer analysis of conical pin configurations in jet impingement cooling with elongated nozzle holes. J Taiwan Inst Chem Eng 164
12. Yalçınkaya O, Durmaz U, Tepe AÜ et al (2023) Assessment of convective heat transfer characteristics for Elliptical-Shaped Pin-Roughened surface for the jet impingement cooling. ASME J Heat Mass Transf 145
13. Jambunathan K, Lai E, Moss MA, Button BL (1992) A review of heat transfer data for single circular jet impingement. Int J Heat Fluid Flow 13:106–115. https://doi.org/10.1016/0142-727X(92)90017-4
14. Yalçınkaya O, Durmaz U, Tepe AÜ et al (2024) Heat and flow characteristics of Aerofoil-Shaped fins on a curved target surface in a confined channel for an impinging jet array. Energies 17. https://doi.org/10.3390/en17051238

15. Shukla AK, Dewan A (2017) Flow and thermal characteristics of jet impingement: comprehensive review. Int J Heat Technol 35:153–166. https://doi.org/10.18280/ijht.350121

16. Rasheed A, Allauddin U, Ali HM et al (2022) Heat transfer and fluid flow characteristics investigation using detached ribs in an axisymmetric impinging jet flow. J Therm Anal Calorim 147:14517–14537. https://doi.org/10.1007/s10973-022-11640-w

17. Liou TM, Wang W, Bin, Chang YJ (1995) Holographic interferometry study of spatially periodic heat transfer in a channel with ribs detached from one wall. J Heat Transf 117:32–39. https://doi.org/10.1115/1.2822319

18. Dewan A, Gupt DP, Sanghi S (2013) Enhancement of heat transfer through jet impingement by using detached ribs. Int Rev Mech Eng 7:308–317

19. Celik N (2011) Effects of the surface roughness on heat transfer of perpendicularly impinging co-axial jet. Heat Mass Transf Und Stoffuebertragung 47:1209–1217. https://doi.org/10.1007/s00231-011-0785-9

20. Chung HS, Lee GH, Nine MJ et al (2014) Study on the thermal and flow characteristics on the periodically arranged semi-circular ribs in a rectangular channel. Exp Heat Transf 27:56–71. https://doi.org/10.1080/08916152.2012.719067

21. Brakmann R, Chen L, Poser R et al (2019) Heat transfer investigation of an array of jets impinging on a target plate with detached ribs. Int J Heat Fluid Flow 78:108420. https://doi.org/10.1016/j.ijheatfluidflow.2019.05.009

22. Katti V, Prabhu SV (2008) Heat transfer enhancement on a flat surface with axisymmetric detached ribs by normal impingement of circular air jet. Int J Heat Fluid Flow 29:1279–1294. https://doi.org/10.1016/j.ijheatfluidflow.2008.05.003

23. Adimurthy M, Venkatesha, Vadiraj VK (2016) Experimental study of fluid flow and heat transfer characteristics of rough surface, impinged by a confined laminar slot air jet. Int J Eng Res V5. https://doi.org/10.17577/ijertv5is060418

24. Alenezi AH, Almutairi A, Alhajeri HM et al (2018) Flow structure and heat transfer of jet impingement on a rib-roughened flat plate. Energies 11. https://doi.org/10.3390/en11061550

25. Katti V, Prabhu SV (2008) Experimental study and theoretical analysis of local heat transfer distribution between smooth flat surface and impinging air jet from a circular straight pipe nozzle. Int J Heat Mass Transf 51:4480–4495. https://doi.org/10.1016/j.ijheatmasstransfer.2007.12.024

26. Moffat RJ (1988) Describing the uncertainties in experimental results. Exp Therm Fluid Sci 1:3–17. https://doi.org/10.1016/0894-1777(88)90043-X

27. Abdul AA, Jirunthanin V, Hamad FA (2014) Numerical and experimental study of flow structure and cooling behavior of air impingement on a target plate. Int J Therm Environ Eng 08. https://doi.org/10.5383/ijtee.08.01.005

28. Schlichting H, Gersten K (2016) Boundary-Layer theory. Springer Berlin, Berlin Heidelberg

29. Zuckerman N, Lior N (2006) Jet impingement heat transfer: physics, correlations, and numerical modeling. Elsevier Masson SAS

30. Maghrabie HM (2021) Heat transfer intensification of jet impingement using exciting jets - A comprehensive review. Renew Sustain Energy Rev 139:110684. https://doi.org/10.1016/j.rser.2020.110684

31. Saric WS, Reed HL, Kerschen EJ (2002) Boundary-layer receptivity to freestream disturbances. Annu Rev Fluid Mech 34:291–319. https://doi.org/10.1146/annurev.fluid.34.082701.161921

32. Kadivar M, Tormey D, McGranaghan G (2021) A review on turbulent flow over rough surfaces: fundamentals and theories. Int J Thermofluids 10:100077. https://doi.org/10.1016/j.ijft.2021.100077

33. Hadipour A, Rajabi Zargarabadi M, Mohammadpour J (2020) Effects of a triangular guide rib on flow and heat transfer in a turbulent jet impingement on an asymmetric concave surface. Phys Fluids 32. https://doi.org/10.1063/5.0010480

34. Allauddin U, Uddin N, Weigand B (2013) Heat transfer enhancement by jet impingement on a flat surface with detached-ribs under cross-flow conditions. Numer Heat Transf Part Appl 63:921–940. https://doi.org/10.1080/10407782.2013.757155